

# Information-entropic measures for non-zero $l$ states of confined hydrogen-like ions

Neetik Mukherjee\* and Amlan K. Roy†

*Department of Chemical Sciences*

*Indian Institute of Science Education and Research (IISER) Kolkata,*

*Mohanpur-741246, Nadia, WB, India*

## Abstract

Rényi entropy ( $R$ ), Tsallis entropy ( $T$ ), Shannon entropy ( $S$ ), and Onicescu energy ( $E$ ) are studied in a spherically confined H atom (CHA), in conjugate space, with special emphasis on non-zero  $l$  states. **This work is a continuation of our recently published work [1].** Representative calculations are done by employing *exact* analytical wave functions in  $r$  space. Accurate  $p$  space-wave functions are generated numerically by performing Fourier transform on respective  $r$ -space counterparts. Further, these are extended for H-isoelectronic series by applying the scaling relations.  $R, T$  are evaluated by choosing the order of entropic moments  $(\alpha, \beta)$  as  $(\frac{3}{5}, 3)$  in  $r$  and  $p$  spaces. Detailed, systematic results of all these measures with respect to variations of confinement radius  $r_c$  are offered here for arbitrary  $n, l$  quantum numbers. For a given  $n$ , at small  $r_c$ ,  $R_{\mathbf{r}}^{\alpha}, T_{\mathbf{r}}^{\alpha}, S_{\mathbf{r}}$  collapse with rise of  $l$ , attain a minimum, then again grow up. Growth in  $r_c$  shifts the point of inflection towards higher  $l$  values. An increase in  $Z$  enhances localization of a particular state. Several other new interesting inferences are uncovered. Comparison with literature results (available only for  $S$  in  $2p, 3d$  states), offers excellent agreement.

**PACS:** 03.65-w, 03.65Ca, 03.65Ta, 03.65.Ge, 03.67-a.

**Keywords:** Rényi entropy, Shannon entropy, Onicescu energy, Tsallis entropy, Confined hydrogen atom, Scaling relation.

---

\*Email: neetik.mukherjee@iiserkol.ac.in.

†Corresponding author. Email: akroy@iiserkol.ac.in, akroy6k@gmail.com.

## I. INTRODUCTION

Confinement of an atom or molecule inside an impenetrable cavity was first studied in the fourth decade of twentieth century [2]. Progress of research on such quantum systems was reviewed several times [2–5] recording their importance in both fundamental physics and chemistry as well as in various engineering branches. They have relevance in many different physical situations, e.g., atoms under plasma environment, impurities in crystal lattice and semiconductor materials, trapping of atoms/molecules in zeolite cages or inside an endohedral cobweb of fullerenes, quantum wells, quantum wires, quantum dots [6] and so forth. Furthermore, such models were designed to mimic the high pressure environment inside the core of planets. Also, they have contemporary significance in interpreting various astrophysical phenomena [7] and many other interesting areas.

Theoretical study of a Hydrogen atom within an infinite spherical cavity was first published in 1937 [8]. Over the years, this simple confined hydrogen atom (CHA) model has served as a precursor to improve our understanding about the consequences of confinement in atomic electronic structure. In last decade, a CHA under the influence of various restricted environment has been extensively followed. Majority of these investigations include trapping of H atom either in a spherical box of penetrable, impenetrable walls or inside a hard box of different geometrical shape and size [5, 9–12]. In the realm of atomic physics, CHA provides us with many attractive physical and chemical properties. Numerous theoretical methods like perturbation theory, Padé approximation, WKB method, Hypervirial theorem, power-series solution, Lie algebra, Lagrange-mesh method, asymptotic iteration method, generalized pseudo-spectral (GPS) method were invoked for their proper treatment. Many interesting aspects such as rearrangement and redistribution of ground and excited energy states, *simultaneous* and *incidental* degeneracy, change in hyperfine splitting constant as well as dipole shielding factor, nuclear magnetic screening constant, pressure, variation of static and dynamic polarizability, hyperpolarizability, information entropy, etc., were probed with varying confining radius ( $r_c$ ). A vast literature exists on the subject; here we refer to a selective set [13–24]. Eigenvalues and eigenfunctions of CHA can be solved *exactly* in terms of Kummer M-function (confluent hypergeometric) [17].

In past twenty years, information measures were explored extensively for various quantum systems in both free and confinement situations. Some such potentials are: Pöschl-Teller

[25], Rosen-Morse [26], pseudo-harmonic [27], squared tangent well [28], hyperbolic [29], position-dependent mass Schrödinger equation [30, 31], infinite circular well [32], hyperbolic double-well (DW) potential [33], etc. Recently, entropic measures were successfully engaged to understand trapping and oscillation of a particle within symmetric, asymmetric DW potential [34, 35], confined quantum harmonic oscillator [36], CHA [9, 10], etc.

Information-theoretic measures like Rényi entropy ( $R$ ), Tsallis entropy ( $T$ ), Shannon entropy ( $S$ ) and Onicescu energy ( $E$ ), in atomic systems may provide detailed knowledge about diffusion of atomic orbitals, spread of electron density, periodic properties, correlation energy and so forth [37–40].  $R, T$ , called information generating functionals, are directly connected to *entropic moments* and completely quantify density. Former has been effectively employed to illustrate quantum entanglement, chemical reactivity, de-coherence and localization properties of Rydberg states of atoms [41–47]. Similarly,  $T$  has been implicated specially for non-extensive thermo-statistics [48, 49] and gravitation [50, 51], etc. It is noteworthy that,  $S, E$  are two special cases of  $R, T$ . Former measures extent of concentration of the system wave function in respective space, whereas latter symbolizes expectation values of density.  $S$  has its application in illuminating colin conjecture, atomic avoided crossing, orbital free density functional theory [52–56] in many-electron systems, etc. Likewise,  $E$  has been widely used to estimate correlation energy and first ionisation potential [40].

In past few years appreciable attention has been paid to explore  $S$  in both  $r$  and  $p$  space for CHA under soft and hard confinement [9]. Very recently,  $S$  in conjugate space has been examined (for low-lying  $s, p, d$  orbitals) with the help of variation principle employing Slater type orbitals [10]. However, rest of the information measures like  $R, T, E$  have been attempted very rarely, with the exception of some first few  $s$ -states of CHA [1]. Hence, our primary motivation is to undertake a detailed analysis of  $R, T, S, E$  in a CHA-like system in a systematic fashion for an arbitrary state characterized by principal and azimuthal quantum numbers  $n, l$ , in both spaces, with special emphasis on  $l \neq 0$ . Illustrative calculations are performed with *exact* analytical wave functions in  $r$ -space; whereas in  $p$  space, numerical wave functions are generated by executing Fourier transform on the eigenfunction of respective  $r$ -space orbitals. To put things in proper perspective, in this communication,  $2p, 3d, 4f, 5g$  and  $10s-10m$  states have been chosen as representatives. By considering all the acceptable  $l$ 's corresponding to a given  $n$ , one can follow the changes in behavior of  $l$  states as the environment switches from *free* to *confinement*. Such a comparative study

of these information measures are done with respect to their free Hydrogen atom (FHA) counterpart. We also inspect the nature of  $R, T, S, E$  for hydrogenic isoelectronic series (by varying atomic number  $Z$ ) inside the spherical impenetrable cavity, using the scaling properties [57] satisfied by such a system. This time we restrict ourselves to ground state only; for extension to other states is straightforward. To this end, all measures in a CHA-like atoms are obtained in both  $r, p$  and composite spaces. Note that such studies in a CHA are very rare and as already implied, most of the present results are offered here for the first time. Throughout the article, comparison with existing literature results are made wherever possible. Organization of this article is as follows. Section II gives a brief account of the theoretical method used; Sec. III presents a detailed discussion on the results of  $R, T, S, E$  of CHA and H-isoelectronic series, while we conclude with a few remarks in Sec. IV.

## II. THEORETICAL METHOD

The time-independent, non-relativistic radial Schrödinger equation under the influence of confinement, without loss of generality, for a central potential, may be written as,

$$\left[ -\frac{1}{2} \frac{d^2}{dr^2} + \frac{\ell(\ell+1)}{2r^2} + v(r) + v_c(r) \right] \psi_{n,\ell}(r) = \mathcal{E}_{n,\ell} \psi_{n,\ell}(r), \quad (1)$$

where  $v(r) = -\frac{Z}{r}$  ( $Z$  implies atomic number). Our desired effect of radial confinement inside an impenetrable hard cavity can be modeled by invoking the following form of potential:  $v_c(r) = +\infty$  for  $r > r_c$  and 0 for  $r \leq r_c$ , where  $r_c$  corresponds to radius of the cage. It is worthwhile mentioning that, atomic units are employed through out the calculations and  $\mathbf{r}, \mathbf{p}$  subscripts denote quantities in full  $r$  and  $p$  spaces (including the angular part) respectively.

On solving Eq. (1) one can obtain following *exact* form for eigenfunctions in CHA [17],

$$\psi_{n,l}(Zr) = N_{n,l} \left( 2Zr\sqrt{-2\mathcal{E}_{n,l}} \right)^l {}_1F_1 \left[ \left( l+1 - \frac{1}{\sqrt{-2\mathcal{E}_{n,l}}} \right), (2l+2), 2Zr\sqrt{-2\mathcal{E}_{n,l}} \right] e^{-Zr\sqrt{-2\mathcal{E}_{n,l}}}. \quad (2)$$

Here,  $N_{n,l}$  represents the normalization constant,  $\mathcal{E}_{n,l}$  prevails to energy of a given  $n, l$  state while  ${}_1F_1[a, b, r]$  refers to confluent hypergeometric function. Allowed energies at a given  $r_c$  can be retrieved by applying the Dirichlet boundary condition that  $\psi_{n,\ell}(0) = \psi_{n,\ell}(r_c) = 0$  and finding the zeros of  ${}_1F_1$ , such that,

$${}_1F_1 \left[ \left( l+1 - \frac{1}{\sqrt{-2\mathcal{E}_{n,l}}} \right), (2l+2), 2Zr_c\sqrt{-2\mathcal{E}_{n,l}} \right] = 0. \quad (3)$$

For a particular  $l$ , first root signifies energy of the lowest state having ( $n_{lowest} = l+1$ ), and consecutive roots imply excited states. Note that, for construction of exact wave function of CHA for a specific state, one needs to provide the energy eigenvalue of that state. In our present calculation,  $\mathcal{E}_{n,l}$  of CHA are computed by invoking the GPS [23] method. This is applied, because in this pursuit, we are interested in the information measures in CHA, for which GPS energies have been found to be sufficiently accurate to provide correct eigenvalues and eigenfunctions. Over the years, this has been tested in a varied case of important model and realistic potentials, including both *free and confinement* situations [23, 58–60]. Also, it is obvious from Eq. (2) that,  $\mathcal{E}_{n,l}$  depends on the product  $Zr_c$ . Hence in spite of changes in  $Z$  and  $r_c$  separately, if their product remains constant, then  $\mathcal{E}_{n,l}$  will not be affected.

The angular part has following common form in both  $r$  and  $p$  spaces ( $P_l^m(\cos \theta)$  signifies usual associated Legendre polynomial),

$$Y_{l,m}(\Omega) = \Theta_{l,m}(\theta) \Phi_m(\phi) = (-1)^m \sqrt{\frac{2l+1}{4\pi} \frac{(l-m)!}{(l+m)!}} P_l^m(\cos \theta) e^{-im\phi}. \quad (4)$$

The  $p$ -space wave function ( $\mathbf{p} = \{p, \Omega\}$ ) for a particle in a central potential is obtained from respective Fourier transform of its  $r$ -space counterpart, and as such, is given below,

$$\begin{aligned} \psi_{n,l}(p) &= \frac{1}{(2\pi)^{\frac{3}{2}}} \int_0^{r_c} \int_0^\pi \int_0^{2\pi} \psi_{n,l}(r) \Theta(\theta) \Phi(\phi) e^{ipr \cos \theta} r^2 \sin \theta \, dr d\theta d\phi, \\ &= \frac{1}{2\pi} \sqrt{\frac{2l+1}{2}} \int_0^{r_c} \int_0^\pi \psi_{n,l}(r) P_l^0(\cos \theta) e^{ipr \cos \theta} r^2 \sin \theta \, dr d\theta. \end{aligned} \quad (5)$$

Note that, here  $\psi(p)_{n,l}$  needs to be normalized. Integrating over  $\theta$  and  $\phi$  variables, Eq. (5) may be further rewritten as given below,

$$\psi_{n,l}(p) = (-i)^l \int_0^{r_c} \frac{\psi_{n,l}(r)}{p} f(r, p) dr. \quad (6)$$

Depending on  $l$ ,  $f(r, p)$  can be expressed in following simplified form ( $m'$  starts with 0),

$$\begin{aligned} f(r, p) &= \sum_{k=2m'+1}^{m' < \frac{l}{2}} a_k \frac{\cos pr}{p^k r^{k-1}} + \sum_{j=2m'}^{m' = \frac{l}{2}} b_j \frac{\sin pr}{p^j r^{j-1}}, \quad \text{for even } l, \\ f(r, p) &= \sum_{k=2m'}^{m' = \frac{l-1}{2}} a_k \frac{\cos pr}{p^k r^{k-1}} + \sum_{j=2m'+1}^{m' = \frac{l-1}{2}} b_j \frac{\sin pr}{p^j r^{j-1}}, \quad \text{for odd } l. \end{aligned} \quad (7)$$

The coefficients  $a_k$ ,  $b_j$  of even- $l$  and odd- $l$  states are calculated using Eq. (5).

Let  $\rho(\mathbf{r})$  and  $\Pi(\mathbf{p})$  denote normalized position and momentum electron densities for CHA. Then, position, momentum shannon entropies ( $S_{\mathbf{r}}, S_{\mathbf{p}}$ ) and their sum ( $S_t$ ) for H-like atoms are defined in terms of expectation values of logarithmic probability density functions and  $Z$ , which for a central potential further simplify to,

$$\begin{aligned} S_{\mathbf{r}}(Z) &= -3 \ln Z + S_{\mathbf{r}}(Z = 1), & S_{\mathbf{p}}(Z) &= 3 \ln Z + S_{\mathbf{p}}(Z = 1) \\ S_{\mathbf{r}}(Z = 1) &= - \int_{\mathcal{R}^3} \rho(\mathbf{r}) \ln[\rho(\mathbf{r})] d\mathbf{r}, & S_{\mathbf{p}}(Z = 1) &= - \int_{\mathcal{R}^3} \Pi(\mathbf{p}) \ln[\Pi(\mathbf{p})] d\mathbf{p} \\ S_t &= S_{\mathbf{r}}(Z) + S_{\mathbf{p}}(Z) = S_{\mathbf{r}}(Z = 1) + S_{\mathbf{p}}(Z = 1) \end{aligned} \quad (8)$$

The above equation clearly suggests that, at a fixed  $r_c$ , both  $S_{\mathbf{r}}(Z)$  and  $S_{\mathbf{p}}(Z)$  are linear functions of logarithm of  $Z$  with slope  $-3$  and  $3$  respectively. Moreover,  $S_{\mathbf{r}}(Z = 1)$ ,  $S_{\mathbf{p}}(Z = 1)$  act as intercepts in  $r$ - and  $p$ -space equations. The last equation implies that addition of  $S_{\mathbf{r}}(Z)$  and  $S_{\mathbf{p}}(Z)$  produces same result as one obtains from the corresponding sum for  $Z = 1$ . Hence  $S_t$  will remain unaltered with change in  $Z$ . Actually it has been established [57] that it solely depends on  $Zr_c$  product as evident from Eq. (3), rather than individual  $Z$  and  $r_c$ . Here and in the discussion throughout the article,  $Z$  dependence is identified in the parentheses of all respective measures, for  $Z > 1$ . For CHA ( $Z = 1$ ), there are no parentheses in the expressions of  $R, T, S, E$ .

Similarly, Rényi entropies of order  $\lambda (\neq 1)$  are obtained by taking logarithm of  $\lambda$ -order entropic moment. In spherical polar coordinate, they are expressed as,

$$\begin{aligned} R_{\mathbf{r}}^{\lambda}(Z = 1) &= \frac{1}{1 - \lambda} \ln \left( \int_{\mathcal{R}^3} \rho^{\lambda}(\mathbf{r}) d\mathbf{r} \right) = \frac{1}{(1 - \lambda)} \ln \left( 2\pi \int_0^{\infty} [\rho(r)]^{\lambda} r^2 dr \int_0^{\pi} [\chi(\theta)]^{\lambda} \sin \theta d\theta \right) \\ &= \frac{1}{(1 - \lambda)} (\ln 2\pi + \ln[\omega_r^{\lambda}] + \ln[\omega_{(\theta, \phi)}^{\lambda}]), \\ R_{\mathbf{p}}^{\lambda}(Z = 1) &= \frac{1}{1 - \lambda} \ln \left[ \int_{\mathcal{R}^3} \Pi^{\lambda}(\mathbf{p}) d\mathbf{p} \right] = \frac{1}{(1 - \lambda)} \ln \left( 2\pi \int_0^{\infty} [\Pi(p)]^{\lambda} p^2 dp \int_0^{\pi} [\chi(\theta)]^{\lambda} \sin \theta d\theta \right) \\ &= \frac{1}{(1 - \lambda)} (\ln 2\pi + \ln[\omega_p^{\lambda}] + \ln[\omega_{(\theta, \phi)}^{\lambda}]). \end{aligned} \quad (9)$$

where  $\omega_{\tau}^{\lambda}$ 's are entropic moments in  $\tau$  ( $r$  or  $p$  or  $\theta, \phi$ ) space with order  $\lambda$ , having forms,

$$\omega_r^{\lambda} = \int_0^{\infty} [\rho(r)]^{\lambda} r^2 dr, \quad \text{ersta6.tex} \omega_p^{\lambda} = \int_0^{\infty} [\Pi(p)]^{\lambda} p^2 dp, \quad \omega_{(\theta, \phi)}^{\lambda} = \int_0^{\pi} [\chi(\theta)]^{\lambda} \sin \theta d\theta. \quad (10)$$

Here if  $\lambda$  corresponds to  $\alpha, \beta$  in  $r, p$  spaces respectively, then they are related as  $\frac{1}{\alpha} + \frac{1}{\beta} = 2$ .

In that case, one can define Rényi entropy sum as,

$$R_t^{(\alpha,\beta)} = \frac{2 - \alpha - \beta}{(1 - \alpha)(1 - \beta)} \ln 2\pi + \frac{1}{(1 - \alpha)} (\ln[\omega_r^\alpha] + \ln[\omega_{(\theta,\phi)}^\alpha]) + \frac{1}{(1 - \beta)} (\ln[\omega_p^\beta] + \ln[\omega_{(\theta,\phi)}^\beta]). \quad (11)$$

Equation (9) suggests that, at a particular  $r_c$ , like  $S_r(Z)$ ,  $S_p(Z)$ , both  $R_r^\lambda(Z)$  and  $R_p^\lambda(Z)$  also linearly depend on  $\ln Z$  (slope  $-3, 3$  respectively) with intercepts  $R_r^\lambda(Z = 1)$  and  $R_p^\lambda(Z = 1)$  respectively. Further, as with  $S_t$ ,  $R^{(\alpha,\beta)}$  also remains unimpacted with change of  $Z$ .

In a similar fashion, Tsallis entropies [61] in  $r, p$  space and their product can be written down as below,

$$\begin{aligned} T_r^\alpha(Z) &= \left( \frac{1}{\alpha - 1} \right) \left[ 1 - \frac{1}{Z^3} \int_{\mathcal{R}^3} \rho^\alpha(\mathbf{r}) d\mathbf{r} \right] = \left( \frac{1}{\alpha - 1} \right) \left[ 1 - \frac{1}{Z^3} \omega_r^\alpha \omega_{(\theta,\phi)}^\alpha \right] \\ T_p^\beta(Z) &= \left( \frac{1}{\beta - 1} \right) \left[ 1 - Z^3 \int_{\mathcal{R}^3} \Pi^\beta(\mathbf{p}) d\mathbf{p} \right] = \left( \frac{1}{\beta - 1} \right) \left[ 1 - Z^3 \omega_r^\beta \omega_{(\theta,\phi)}^\beta \right] \\ T_t^{(\alpha,\beta)}(Z) &= T_r^\alpha(Z) T_p^\beta(Z) \end{aligned} \quad (12)$$

One sees that,  $T_r^\alpha(Z)$  reduces and  $T_p^\beta(Z)$  enhances with rise of  $Z$ . Note that  $\alpha = \beta = 2$  leads to Onicescu energy  $E$ , which in  $r$  and  $p$  spaces are given as,

$$\begin{aligned} E_r(Z) &= Z^3 \omega_r^2 \omega_{(\theta,\phi)}^2 = Z^3 E_r(Z = 1) \\ E_p(Z) &= \frac{1}{Z^3} \omega_r^2 \omega_{(\theta,\phi)}^2 = \frac{1}{Z^3} E_p(Z = 1) \\ E_t(Z) &= E_r(Z) E_p(Z) = E_r(Z = 1) E_p(Z = 1). \end{aligned} \quad (13)$$

Here,  $E_t$  represents onicescu energy product. Dependence of  $E_r(Z)$  and  $E_p(Z)$  on  $Z$  is seen to be opposite to that of the previous three measures discussed above. Thus  $E_r(Z)$  grows up and  $E_p(Z)$  falls off with rise of  $Z$ . But, as usual,  $E_t(Z)$  remains unchanged as  $Z$  modifies.

### III. RESULT AND DISCUSSION

At the outset, it is appropriate to mention a few things regarding the presentation. Here, our focus is to uncover the impact of an impenetrable spherical cage on *non-zero*  $l$  states of CHA by using information-theoretic measures. The *net* information measures in conjugate  $r$  and  $p$  space of CHA may be segmented into two separate contributions, *viz.*, (i) a radial and (ii) an angular part. In CHA, the radial barrier changes from infinity to a finite region without affecting angular boundary conditions. So angular portion remains invariant in  $r$  and  $p$  spaces; moreover they will also not change with respect to boundary

TABLE I: Rényi entropies,  $R_{\mathbf{r}}^{\alpha}$ ,  $R_{\mathbf{p}}^{\beta}$  and  $R_t^{(\alpha,\beta)}$  for  $2p$ ,  $3d$  states of CHA at selected  $r_c$  values, with  $\alpha = \frac{3}{5}$  and  $\beta = 3$ . See text for details.

$r_c$	$R_{\mathbf{r}}^{\alpha}$	$R_{\mathbf{p}}^{\beta}$	$R_t^{(\alpha,\beta)}$	$r_c$	$R_{\mathbf{r}}^{\alpha}$	$R_{\mathbf{p}}^{\beta}$	$R_t^{(\alpha,\beta)}$
$2p^{\dagger}$				$3d^{\P}$			
0.1	-6.16888358521	12.8086549	6.6397714	0.1	-6.11864461237	13.2299266	7.111282
0.2	-4.09121892459	10.7314035	6.6401846	0.2	-4.03973495813	11.1514674	7.1117325
0.3	-2.87663035551	9.5172358	6.6406055	0.3	-2.82387786690	9.9360644	7.1121866
0.5	-1.34785892643	7.9893299	6.641471	0.5	-1.29249680384	8.4056025	7.1131057
0.8	0.05635500373	6.5864754	6.6428304	0.8	0.11582086058	6.9986916	7.1145125
1	0.72175456102	5.9220245	6.643779	1	0.78408877031	6.3313805	7.1154693
5	5.43150144784	1.2403914	6.6718928	7.5	6.77107758150	0.3857834	7.1568610
15	7.78024380659	-0.924233	6.8560108	15	8.69500260562	-1.45238070	7.2426219
25	7.92394945000	-0.9742317	6.9497178	50	9.92580433711	-2.311277606	7.614526731
45	7.92577664624	-0.9736503	6.9521263	100	9.92600859049	-2.311283603	7.614724988

$^{\dagger}R_{\mathbf{r}}^{\alpha}$ ,  $R_{\mathbf{p}}^{\beta}$ ,  $R_t^{(\alpha,\beta)}$  in FHA for  $2p$  states ( $|m| = 0$ ) are: 7.925776675482, -0.9736503771629, 6.952126298319.

$^{\P}R_{\mathbf{r}}^{\alpha}$ ,  $R_{\mathbf{p}}^{\beta}$ ,  $R_t^{(\alpha,\beta)}$  in FHA for  $3d$  states ( $|m| = 0$ ) are: 9.926008594642, -2.311283609195, 7.614724985446.

condition in  $r_c$  in a CHA. However, they will be affected by  $l$ ,  $m$  quantum numbers. In current calculation, we have kept magnetic quantum number  $m$  fixed at 0, unless stated otherwise. It is clear from Eq. (2) that, in  $r$  space, radial wave functions are available in closed analytical form. In  $p$  space, numerical wave functions are achieved by employing Fourier transform on respective  $r$ -space eigenfunctions. All our results provided in tables and figures are computed numerically. It is expected that, a gradual increase in  $r_c$  should lead to a delocalization in the system in such a fashion that, when  $r_c \rightarrow \infty$ , it should unfold to FHA. On the contrary, when  $r_c \rightarrow 0$ , impression of confinement is maximum. Thus, it is convenient to explore our analysis by choosing some specific  $r_c$  values in the range of 0.1 to 100. This parametric rise in  $r_c$  reveals evolution of system from maximum confinement to a free system. It may be remarked that, a detailed systematic analysis of these measures in low-lying  $s$  states, along the lines of current work, has been initiated by present authors and will be published elsewhere [1].

Our presentation strategy is as follows. Initially,  $2p, 3d, 4f, 5g$  states are selected for analysis of various information measures; they all individually represent the lowest (nodeless) state of respective  $l$ . This will help us follow changes in  $R, S, T, E$  with respect to alterations in  $l$ . Additionally we also explore all the  $l$  states corresponding to a given  $n$  (here chosen



TABLE II:  $R_{\mathbf{r}}^{\alpha}$  and  $R_{\mathbf{p}}^{\beta}$  for  $10l$  states of CHA at seven different  $r_c$  values, namely 0.1, 0.5, 1, 10, 40, 80, 100. Here,  $\alpha, \beta$  are chosen to be  $\frac{3}{5}$  and 3 respectively. See text for details.

$R_{\mathbf{r}}^{\alpha}$							
$l$	$r_c = 0.1$	$r_c = 0.5$	$r_c = 1$	$r_c = 10$	$r_c = 40$	$r_c = 80$	$r_c = 100$
0	-6.0792476535	-1.2500151671	0.8305932083	7.7616144459	11.9866555713	14.1264898722	14.8227228363
1	-6.3891801965	-1.5604409325	0.5195411162	7.4386341260	11.6485744296	13.7938994865	14.4924250904
2	-6.3886059693	-1.5600883216	0.5196127247	7.4330589592	11.6242072771	13.7633595572	14.4630426402
3	-6.3665110491	-1.5381245479	0.5414121420	7.4515237538	11.6283879357	13.7541478868	14.4519363360
4	-6.3359608527	-1.5076548776	0.5717793565	7.4797957142	11.6465100421	13.7573382983	14.4505385080
5	-6.2994173707	-1.4711571510	0.6082191748	7.5150095855	11.6749072268	13.7721369041	14.4592392391
6	-6.2581496967	-1.4299022978	0.6494567192	7.5558021952	11.7119190030	13.7982974268	14.4788958301
7	-6.2143631650	-1.3860901364	0.6933001405	7.6001063439	11.7558856869	13.8354493928	14.5099982856
8	-6.1748354691	-1.3464778435	0.7330180632	7.6416699182	11.8023199187	13.8818610231	14.5518827831
9	-6.1702611858	-1.3416902256	0.7380727967	7.6515945538	11.8288561033	13.9252706635	14.5938547362
$R_{\mathbf{p}}^{\beta}$							
0	17.764042	12.938472	10.863484	4.225406	-0.104732	-2.194616	-3.015142
1	16.990848	12.164511	10.087976	3.319124	-0.643120	-2.666435	-3.423219
2	16.609713	11.782989	9.705776	2.886201	-0.749884	-2.917930	-3.674227
3	16.31713	11.490168	9.412558	2.566775	-1.040808	-3.221412	-3.822730
4	16.059368	11.2322271	9.154340	2.292588	-1.439844	-3.385452	-4.054590
5	15.8154003	10.9881122	8.910008	2.037463	-1.820272	-3.487284	-4.250016
6	15.573099	10.745675	8.667378	1.786891	-2.166955	-3.735834	-4.383047
7	15.322708	10.495141	8.416651	1.529727	-2.494875	-4.1772092	-4.645285
8	15.052818	10.225072	8.146348	1.253299	-2.824948	-4.672206	-5.156688
9	14.7302406	9.9021894	7.823079	0.9218974	-3.204373	-5.196718	-5.787983

10) to understand the outcome as the count of radial nodes vary. Actually, for a given  $l$ , an increase in  $n$  enhances spreading as well as number of radial nodes, whereas an increment in  $l$  within in a given  $n$  reduces radial node.

To begin with, Table I displays our calculated  $R_{\mathbf{r}}^{\alpha}, R_{\mathbf{r}}^{\alpha}, R_t^{(\alpha, \beta)}$  for  $2p, 3d$  states of CHA at a selected set of  $r_c$ ; which differ from state to state. Similarly, Table S1 in supplementary material (SM) portrays all the above quantities as a function of  $r_c$  for  $4f, 5g$  states. In this and all following tables related to these four states, information quantities are provided at *same* set including ten  $r_c$ 's. In all occasions,  $R_{\mathbf{r}}^{\alpha}$ 's progress continuously with  $r_c$  and finally converge to respective FHA behavior after some larger finite  $r_c$ . Interestingly, for all states,  $R_{\mathbf{r}}^{\alpha}$  remain negative up to  $r_c = 0.5$ , changing sign after that. In contrast,  $R_{\mathbf{p}}^{\beta}$ 's, tend to diminish with rise of  $r_c$ ; eventually they also merge to FHA (negative for all) in the end. As a combination of these two effects,  $R^{(\alpha, \beta)}$ 's steadily grow with progress of  $r_c$  and as usual

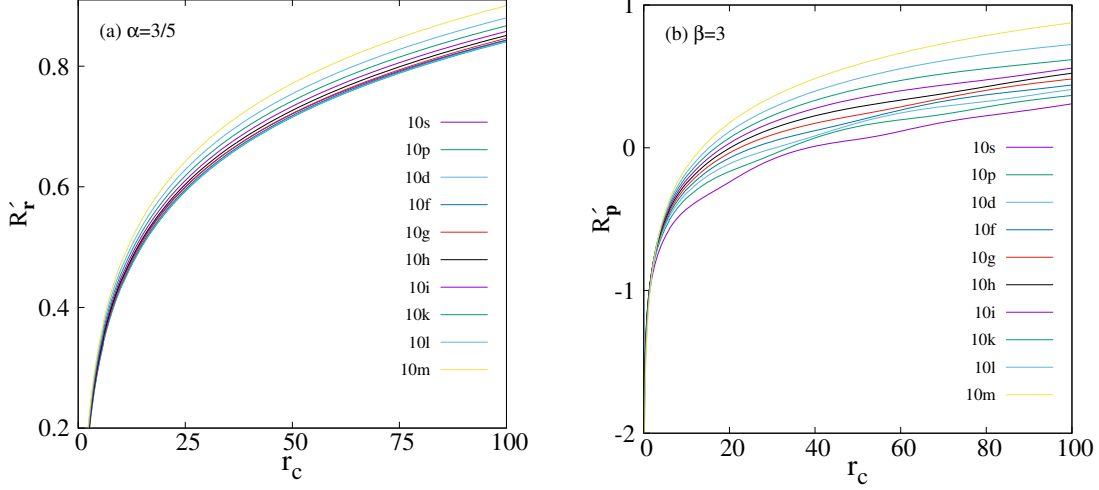


FIG. 1: Variation of  $R'_r, R'_p$  with  $r_c$  for 10s–10m states of CHA in panels (a), (b).  $\alpha, \beta$  are chosen to be  $\frac{3}{5}$  and 3 respectively. See text for detail.

they coalesce to respective borderline values finally. It is worth mentioning that, at *small*  $r_c$ , Rényi entropies in  $r, p$  space obey same order:  $R'_r(5g) > R'_r(4f) > R'_r(3d) > R'_r(2p)$  and  $R'_p(5g) > R'_p(4f) > R'_p(3d) > R'_p(2p)$ . But, at  $r_c \rightarrow \infty$  limit, ordering in  $p$  space completely reverses, while the  $r$ -space ordering is retained. The distribution pattern in  $r$  space is observed presumably because, an increase in both  $n, l$  leads to more delocalization of CHA. Next Table II provides  $R'_r, R'_p$  for all states having  $l = 0 - 9$ , within  $n = 10$  of CHA, at seven selected  $r_c$ , namely 0.1, 0.5, 1, 10, 40, 80, 100, featuring strong to medium confinement. At smaller  $r_c$  ( $< 1$ ) region,  $R'^\alpha_r$ 's remain (–)ve for all ten  $l$ ; for rest five  $r_c$  ( $> 1$ ), the sign reverses. Numerical values surge with  $r_c$  for all  $l$ . In all seven instances of  $r_c$ ,  $R'^\alpha_r$ 's initially fall as  $l$  increments, then attain a minimum for some  $l$  and again go up. **In first three  $r_c$  (0.1, 0.5, 1) these minima occur at  $l = 1$ . At  $r_c = 10, 40$  these happen at  $l = 2$ . Further, These minima shift to  $l = 3$  and  $l = 4$  for  $r_c = 80$  and 100 respectively.** In contrast, numerical values of  $R'^\beta_p$  gradually lower with growth of  $r_c$  for each  $l$ . Furthermore, in all seven  $r_c$ , it falls down with  $l$  without going through any inflection points unlike its corresponding  $r$ -space counterpart. To the best of our knowledge, no such results have been reported for Rényi entropy in CHA. Hence they could not be directly compared, and hopefully would provide useful guidelines for future work.

Above changes of Table II are depicted in Fig. 1 in the form of ratios  $R'_r = \left( \frac{R^\alpha_r(\text{CHA})}{R^\alpha_r(\text{FHA})} \right)$  and  $R'_p = \left( \frac{R^\beta_p(\text{CHA})}{R^\beta_p(\text{FHA})} \right)$  for all  $l$  states of  $n = 10$ . For convenience, Rényi entropies of CHA, in both spaces, in this occasion, are divided by their respective FHA values. First it is

TABLE III: Tsallis entropies  $T_{\mathbf{r}}^{\alpha}$ ,  $T_{\mathbf{p}}^{\beta}$  and  $T^{(\alpha,\beta)}$  for  $2p$ ,  $3d$  states of CHA at various  $r_c$ , for  $\alpha, \beta$  as  $\frac{3}{5}$  and 3 respectively. For more details, see text.

$r_c$	$T_{\mathbf{r}}^{\alpha}$	$T_{\mathbf{p}}^{\beta}$	$T_t^{(\alpha,\beta)}$	$r_c$	$T_{\mathbf{r}}^{\alpha}$	$T_{\mathbf{p}}^{\beta}$	$T_t^{(\alpha,\beta)}$
$2p^{\dagger}$				$3d^{\P}$			
0.1	-2.2880198630	0.4999999999	-1.1440099313	0.1	-2.28371690687	0.49999999998	-1.1418584534
0.2	-2.0133435459	0.4999999997	-1.0066717723	0.2	-2.00321763758	0.499999999896	-1.0016088186
0.3	-1.7089241387	0.4999999972	-0.8544620646	0.3	-1.69205429127	0.499999998828	-0.8460271437
0.5	-1.0418811277	0.4999999425	-0.5209405039	0.5	-1.00923112502	0.499999974999	-0.5046155373
0.8	0.0569949807	0.4999990493	0.0284974362	0.8	0.11854567062	0.499999583146	0.0592727859
1	0.8367342402	0.4999964094	0.4183641157	1	0.92097719569	0.499998416555	0.4604871395
5	19.452725733	0.4581611514	8.9124832214	7.5	35.0142839008	0.268855906272	9.4137970306
15	53.670306013	-2.6750355	-143.5699738	15	78.4872531785	-8.630443042	-677.379768
25	56.993705192	-3.0089477	-171.4910836	50	130.0039513800	-50.37685125	-6549.18972146
45	57.037203756	-3.0048699	-171.38938035	100	130.0147775743	-50.37746147	-6549.81444873

$^{\dagger}T_{\mathbf{r}}^{\alpha}$ ,  $T_{\mathbf{p}}^{\beta}$ ,  $T^{(\alpha,\beta)}$  in FHA for  $2p$  states ( $|m| = 0$ ) are: 57.037204453034, -3.0048705041661, -171.38941330101483.

$^{\P}T_{\mathbf{r}}^{\alpha}$ ,  $T_{\mathbf{p}}^{\beta}$ ,  $T^{(\alpha,\beta)}$  in FHA for  $3d$  states ( $|m| = 0$ ) are: 130.014775913339, -50.377462107980, -6549.814447051782.

relevant to recall the following facts about these two relative quantities. For any given  $n, l$   $R_{\mathbf{r}}^{\alpha}$  enhances and  $R_{\mathbf{p}}^{\beta}$  declines with rise of  $r_c$ , whereas for a FHA, they assume maximum and minimum values. Further, this minimum in the latter has negative sign. Such a division by their respective free counterpart makes these quantities unit-less and keeps upper bound to unity. This facilitates to observe a similar trend for two conjugate measures as  $r_c$  varies. Simultaneous escalation of both the ratios with increment of  $r_c$  suggests delocalization in the system. Further, unlike Table II, there is hardly any crossover among these  $R'_{\mathbf{r}}$  and  $R'_{\mathbf{p}}$  of  $10l$  states (there were crossovers in  $R_{\mathbf{r}}^{\alpha}$  in Table II). More importantly, throughout the entire range of  $r_c$ , two ratios reduce with growth in  $l$ . This apparently indicates that states with greater number of nodes, experience the effects of confinement to a larger extent. Finally, in the limit of  $r_c \rightarrow \infty$  these quantities for all  $l$  states correspond to *unity*, as expected.

Table III and S2 in SM now report our estimated values of  $T_{\mathbf{r}}^{\alpha}$ ,  $T_{\mathbf{p}}^{\beta}$  and  $T_t^{(\alpha,\beta)}$  for  $2p, 3d$  and  $4f, 5g$  states of CHA successively at the same  $r_c$ 's of Table I and S1. These are carefully selected so as to cover small, moderate and large cavity radius. Once again, there exists no reference work for comparison. In all these four states, starting from some (-)ve value,  $T_{\mathbf{r}}^{\alpha}$ 's advance monotonically with  $r_c$  and finally reach the respective FHA behavior after some larger finite  $r_c$ . Like  $R_{\mathbf{r}}^{\alpha}$  of Table I and S1,  $T_{\mathbf{r}}^{\alpha}$  is also negative up to  $r_c \leq 0.5$ .

TABLE IV: Tsallis entropies  $T_{\mathbf{r}}^{\alpha}$  and  $T_{\mathbf{p}}^{\beta}$  for all  $l$  states corresponding to  $n = 10$ , of CHA at various  $r_c$ , for  $\alpha$  and  $\beta$  as  $\frac{3}{5}$  and 3 respectively. More details can be found in the text.

$l$	$r_c = 0.1$	$r_c = 0.5$	$r_c = 1$	$r_c = 10$	$r_c = 40$	$r_c = 80$	$r_c = 100$
$T_{\mathbf{r}}^{\alpha}$							
0	-2.28028155100	-0.9836825500	0.9852090051	53.2532949166	299.6588765682	708.652348746	937.0301091469
1	-2.30589991419	-1.1607438353	0.5774679920	46.4962802663	261.4396566474	620.0665476461	820.75069711
2	-2.30585532605	-1.1605549274	0.5775561424	46.3871370347	258.8795701728	612.5075565192	811.1316848206
3	-2.30413187694	-1.1487353757	0.6045090554	46.7495501415	259.3170313452	610.2456275455	807.5251254619
4	-2.30172366881	-1.1321655705	0.6424491328	47.3096638083	261.2217971179	611.0280909941	807.072341736
5	-2.29880409954	-1.1120499540	0.6885886895	48.0162247111	264.2344575738	614.6706053311	809.8947988758
6	-2.29545538209	-1.0889560609	0.7416206960	48.8472617617	268.2127601388	621.1627157435	816.3075412867
7	-2.29184130513	-1.0640097551	0.7989716149	49.7653312815	273.0158081039	630.500042316	826.5579416463
8	-2.28852393521	-1.0410753919	0.8518014821	50.6415282666	278.1809736722	642.3612266162	840.5648183275
9	-2.28813664043	-1.0382788056	0.8585853232	50.8529116901	281.1761223672	653.6562832778	854.8383313138
$T_{\mathbf{p}}^{\beta}$							
0	0.499999999999998	0.49999999999	0.4999999998	0.49989313660	-0.116508	-39.789255	-207.416554
1	0.499999999999991	0.49999999998	0.4999999991	0.49934534041	-1.309576	-103.015651	-469.762391
2	0.499999999999981	0.49999999997	0.4999999981	0.49844386357	-1.740324	-170.679518	-776.396253
3	0.499999999999966	0.49999999994	0.4999999966	0.49705220303	-3.508707	-313.589136	-1045.065137
4	0.499999999999944	0.49999999991	0.4999999944	0.49489902295	-8.404357	-435.549958	-1661.925267
5	0.499999999999908	0.49999999985	0.4999999908	0.49150326392	-18.556282	-534.047620	-2456.963057
6	0.499999999999851	0.49999999976	0.4999999851	0.48597521532	-37.620905	-878.267905	-3206.037005
7	0.499999999999754	0.49999999961	0.4999999755	0.47654334855	-72.949846	-2123.956362	-5417.179246
8	0.499999999999579	0.49999999934	0.4999999580	0.45922740769	-141.630950	-5716.873607	-15065.997051
9	0.499999999999197	0.49999999874	0.4999999198	0.42089205609	-303.065930	-16321.820720	-53253.000550

On the contrary, similar to  $R_{\mathbf{p}}^{\beta}$  of Table I and S1, as  $r_c$  progresses,  $T_{\mathbf{p}}^{\beta}$ 's gradually decline from an initial result of  $\approx \frac{1}{2}$ , to large negative values (passing through a zero) at the end to merge with FHA result. Consequently,  $T^{(\alpha,\beta)}$ 's in these circular states grow (starting from a small negative) with advancement of  $r_c$  and then attain a positive maximum and finally fall off to particular FHA value (large negative). As observed for  $R$ ,  $T$ 's in both  $r$ ,  $p$  spaces follow the same order, *viz.*,  $T_{\mathbf{r}}^{\alpha}(5g) > T_{\mathbf{r}}^{\alpha}(4f) > T_{\mathbf{r}}^{\alpha}(3d) > T_{\mathbf{r}}^{\alpha}(2p)$  and  $T_{\mathbf{p}}^{\beta}(5g) > T_{\mathbf{p}}^{\beta}(4f) > T_{\mathbf{p}}^{\beta}(3d) > T_{\mathbf{p}}^{\beta}(2p)$  respectively. As usual, at  $r_c \rightarrow \infty$  the order in  $p$  space reverses to  $T_{\mathbf{p}}^{\beta}(5g) < T_{\mathbf{p}}^{\beta}(4f) < T_{\mathbf{p}}^{\beta}(3d) < T_{\mathbf{p}}^{\beta}(2p)$ . Then we proceed for  $T_{\mathbf{r}}^{\alpha}, T_{\mathbf{p}}^{\beta}$  for  $n = 10$  states at same  $r_c$  of Table II. Similar to  $R_{\mathbf{r}}^{\alpha}$ ,  $T_{\mathbf{r}}^{\alpha}$ 's remain (-)ve for all  $l$  at  $r_c < 1$  and (+)ve for  $r_c > 1$ . For each  $l$ , they increase with  $r_c$ . Again analogous to  $R_{\mathbf{r}}^{\alpha}$ , at each  $r_c$ ,  $T_{\mathbf{r}}^{\alpha}$  first falls down to a minimum and finally grow with  $l$ . For first three  $r_c$ , these minima occur at  $l = 1$ . For  $r_c = 10, 40$  these minima are found at  $l = 2$ , whereas for  $r_c = 40$  and 100 these minima

TABLE V:  $S_r$ ,  $S_p$  and  $S_t$  for  $2p$ ,  $3d$  states of CHA at various  $r_c$ . Reference values [10] for  $2p$  and  $3d$  states quoted here include angular contributions  $S_{(\theta,\phi)}$ , along with  $S_r$  results given in the Supplementary Tables VIII ( $2p$ ) and XIV ( $3d$ ) respectively. See text for details.

$r_c$	$S_r$	$S_p$	$S_t$	$r_c$	$S_r$	$S_p$	$S_t$
$2p^{\ddagger, \S}$				$3d^{\ddagger, \P}$			
0.1	-6.3897304044	13.4182	7.0285	0.1	-6.3559834637	14.0037	7.6477
0.2 <sup>§</sup>	-4.3126791264	11.3396	7.0270	0.2 <sup>†</sup>	-4.2772270811	11.9244	7.6472
0.3	-3.0987163770	10.1240	7.0253	0.3	-3.0615253452	10.7082	7.6467
0.5	-1.5712349891	8.5934	7.0222	0.5	-1.5304613573	9.1761	7.6457
0.8	-0.1690563768	7.1867	7.0177	0.8	-0.1226356677	7.7668	7.6442
1 <sup>§</sup>	0.4949160183	6.5198	7.0147	1 <sup>†</sup>	0.5452929876	7.0980	7.6432
5 <sup>§</sup>	5.1596858896	1.83592	6.9956	7.5	6.5142648552	1.124506	7.63877
15	7.2120252839	0.060324	7.272349	15	8.3843979910	-0.61531257	7.76908542
25	7.2648183351	0.0423328	7.3071511	50 <sup>†</sup>	9.3456307493	-1.232729196	8.1129015533
45	7.2648971157	0.04242079	7.3073179	100 <sup>†</sup>	9.3456341991	-1.232717246	8.112916953

<sup>§</sup>Literature results [10] of  $(S_r, S_p, S_t)$  at  $r_c = 0.2, 1, 5$  in  $2p$  state are:  $(-4.3126791236, 11.3396511782, 7.0269720545)$ ,  $(0.4949160211, 6.5198502152, 7.0147662362)$  and  $(5.1596858926, 1.8359293466, 6.9956152391)$  respectively.

<sup>†</sup>Literature results [10] of  $(S_r, S_p, S_t)$  at  $r_c = 0.2, 1, 50, 100$  in  $3d$  state are:  $(-4.2772270783, 11.9244780687, 6.8797080015)$ ,  $(0.5452929905, 7.098078228, 7.6433712186)$ ,  $(9.3456307877, -1.2327291038, 8.112901684)$ ,

and  $(9.345634202, -1.2327172441, 8.112916958)$  respectively.

<sup>‡</sup>Reference values are added with respective  $S_{(\theta,\phi)}$  values  $(2.0990786249678, 2.0411250061339)$  of  $2p$  and  $3d$  states.

<sup>!</sup> $S_r, S_p, S_t$  in FHA for  $2p$  states ( $|m| = 0$ ) are: 7.264897118452, 0.042420799485, 7.307317917937.

<sup>¶</sup> $S_r, S_p, S_t$  in FHA for  $3d$  states ( $|m| = 0$ ) are: 9.345634202074, -1.232717244109, 8.112916957965.

appear at  $l = 3$  and 4 successively. On the other hand,  $T_p^\beta$  decrease with progress of  $r_c$ . Further, in all seven  $r_c$ ,  $T_p^\beta$ 's consistently decay with  $l$ , although the extent is very less till  $r_c = 1$  and assumes significance only after  $r_c > 5$  or so. As there is a good resemblance of the behavior of CHA and FHA ratios in Rényi and Tsallis entropies in  $r$  and  $p$  spaces, one can expect and predict the qualitative nature of similar plots for  $T$  for these states, and hence omitted here.

Let us now shift our focus on Table V and S3 in SM, where  $S_r, S_p$  and  $S_t$  of CHA are probed for four low-lying circular states corresponding to  $l = 1 - 4$ . The same set of  $r_c$  of Table I and S1 is adopted. This time, a handful of results are available in the literature for  $2p$  (at  $r_c = 0.2, 1, 5$ ) and  $3d$  ( $r_c = 0.2, 1, 50, 100$ ) states of CHA, which are duly quoted. Present results show good agreement with reference data in all occasions.  $S_r, S_p, S_t$  portray analogous behavior to those of  $R_r^\alpha, R_p^\beta$  and  $R^{(\alpha,\beta)}$  respectively. Similar to  $R_r^\alpha$ ,  $S_r$  also take  $(-)$ ve values for all four states at  $r_c < 1$  region and evolve continuously

TABLE VI:  $S_{\mathbf{r}}$  and  $S_{\mathbf{p}}$  for all  $l$  states corresponding to  $n = 10$ , of CHA at representative  $r_c$  values, in top and bottom segments. For more details, consult text.

$l$	$r_c = 0.1$	$r_c = 0.5$	$r_c = 1$	$r_c = 10$	$r_c = 40$	$r_c = 80$	$r_c = 100$
$S_{\mathbf{r}}$							
0	-6.6336010412	-1.8032959712	0.2787117983	7.2442147026	11.5877476335	13.8154049673	14.5452382494
1	-6.9827167662	-2.1537824035	-0.0735403924	6.8533262967	11.1225960687	13.3570558294	14.0927363946
2	-6.9592958229	-2.1308141271	-0.0511509821	6.8629221900	11.0765559826	13.2799996428	14.0148698959
3	-6.8974004176	-2.0691277981	0.0102684892	6.9184633212	11.0999960757	13.2630164065	13.9887469229
4	-6.8231110824	-1.9949407785	0.0843246799	6.9895792871	11.1527172455	13.2805941590	13.9928101925
5	-6.7421222230	-1.9139917010	0.1652222750	7.0691946490	11.2222138846	13.3235593289	14.0216304087
6	-6.6566958653	-1.8285574196	0.2506653439	7.1545675577	11.3032904456	13.3866129318	14.0720358679
7	-6.5693810669	-1.7411860014	0.3381068528	7.2431276172	11.3927769257	13.4664617170	14.1417536426
8	-6.4873245243	-1.6590042222	0.4204449123	7.3282175171	11.4854342953	13.5598715121	14.2284568921
9	-6.4437380685	-1.6151489690	0.4646366944	7.3785621302	11.5570097332	13.6533937166	14.3196849974
$S_{\mathbf{p}}$							
0	18.225	13.399	11.324	4.710	0.711	-1.206	-1.8374
1	17.685	12.858	10.7811	4.0149	0.4927	-1.53	-2.29
2	17.512	12.684	10.6067	3.780	0.308	-1.70	-2.289
3	17.367	12.539	10.461	3.605	-0.032	-1.78	-2.412
4	17.219	12.3919	10.313	3.440	-0.28	-1.872	-2.557
5	17.063	12.2355	10.156	3.270	-0.581	-2.09	-2.6719
6	16.889	12.061	11.982	3.087	-0.875	-2.427	-2.906
7	16.689	12.861	11.782	2.880	-1.171	-2.84	-3.284
8	16.447	12.618	11.539	2.632	-1.482	-3.31	-3.792
9	16.105	12.276	11.197	2.285	-1.871	-3.871	-4.4326

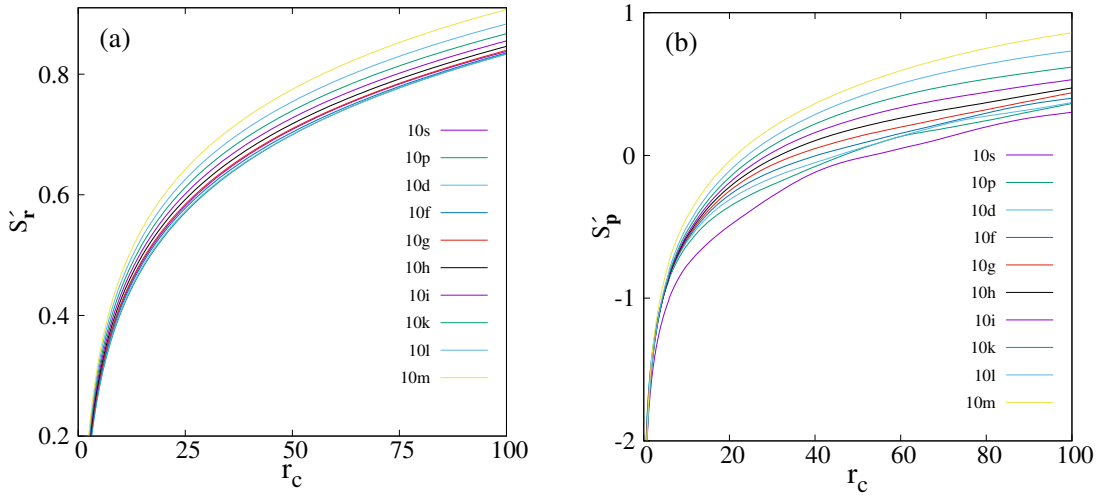


FIG. 2: Variation of  $S'_{\mathbf{r}}$ ,  $S'_{\mathbf{p}}$  of CHA with  $r_c$ , for  $n = 10$  states, in panels (a), (b). See text for detail.

with growth of  $r_c$  before reaching the FHA-limit at large  $r_c$ . On the contrary  $S_{\mathbf{p}}$ , like  $R_{\mathbf{p}}^\beta$ , shows a reverse nature of  $S_{\mathbf{r}}$ .  $S_{\mathbf{p}}$  for  $l = 1 - 4$  ( $n = l + 1$ ) states, starting from (+)ve numerical values, decline as  $r_c$  develops before merging with FHA limit. Consequently,  $S_{\mathbf{r}}$ , falls to reach a minimum and then elevates to attain FHA value. Furthermore,  $S_{\mathbf{r}}$  imprints different pattern to  $R_{\mathbf{r}}^\alpha$  but  $S_{\mathbf{p}}$  delineates similar leaning to  $R_{\mathbf{p}}^\beta$  in smaller  $r_c$ . The observed trend in  $r, p$  spaces is slightly unusual:  $S_{\mathbf{r}}(4f) > S_{\mathbf{r}}(5g) > S_{\mathbf{r}}(3d) > S_{\mathbf{r}}(2p)$  and  $S_{\mathbf{p}}(5g) > S_{\mathbf{p}}(4f) > S_{\mathbf{p}}(3d) > S_{\mathbf{p}}(2p)$  respectively. As usual at  $r_c \rightarrow \infty$  the order in  $r, p$  space reorganize to  $S_{\mathbf{r}}(5g) > S_{\mathbf{r}}(4f) > S_{\mathbf{r}}(3d) > S_{\mathbf{r}}(2p)$  and  $S_{\mathbf{p}}(5g) < S_{\mathbf{p}}(4f) < S_{\mathbf{p}}(3d) < S_{\mathbf{p}}(2p)$ . As a next step, Table VI supplies  $S_{\mathbf{r}}, S_{\mathbf{p}}$  for ten  $l$  states corresponding to  $n = 10$  at same selected  $r_c$  set discussed before.  $S_{\mathbf{r}}$  remains (-)ve for all  $l$  at first two  $r_c$ 's. Interestingly, at  $r_c = 1$ ,  $S_{\mathbf{r}}$  is (-)ve only for  $l = 1, 2$ . In rest of the situation,  $S_{\mathbf{r}}$  takes on (+)ve values.  $S_{\mathbf{r}}$ , in all  $r_c$ 's at first diminish with  $l$ , attain some minima and then gains.  **$S_{\mathbf{r}}$  reaches minimum at  $l = 1$  for first four  $r_c$  values. At  $r_c = 40$  this minimum shifts to  $l = 2$ , whereas for  $r_c = 80$  and 100 these minima arrive at  $l = 3$ .** But in  $p$  space,  $S_{\mathbf{p}}$  imitates  $R_{\mathbf{p}}^\beta$ . Hence, like  $R_{\mathbf{p}}^\beta$ , here  $S_{\mathbf{p}}$  collapses with rise of  $l$ . Here again the nature of  $S_{\mathbf{r}}, S_{\mathbf{p}}$  variation for  $10l$  states remains akin to respective  $R_{\mathbf{r}}^\alpha, R_{\mathbf{p}}^\beta$  changes. Like other states reported here,  $S_{\mathbf{r}}$  progresses and  $S_{\mathbf{p}}$  reduces with growth of  $r_c$ .

Now we move on to Fig. 2 where following the strategy of Fig. 1, the relevant pair of unit-less ratios *viz.*,  $S'_{\mathbf{r}} = \left( \frac{S_{\mathbf{r}}(CHA)}{S_{\mathbf{r}}(FHA)} \right)$  and  $S'_{\mathbf{p}} = \left( \frac{S_{\mathbf{p}}(CHA)}{S_{\mathbf{p}}(FHA)} \right)$  are displayed for all  $l$  states having  $n = 10$ . Drawing reference to Table VI, one notices that, for any given  $n, l$  quantum number,  $S_{\mathbf{r}}$  rises and  $S_{\mathbf{p}}$  falls continuously as  $r_c$  proceeds to reach their corresponding maximum and minimum limits at  $r_c \rightarrow \infty$ . Further, this limiting value in  $S_{\mathbf{p}}$  relates to (-)ve sign (not obvious from Table VI; but further extension of  $r_c$  assures that). Thus both these ratios are bounded to their maximum values to unity. Hence, they both exhibit similar trend in behavior, i.e., grow up with  $r_c$  signifying delocalization of the system. In the entire range of  $r_c$  the values of both  $S'_{\mathbf{r}}$  and  $S'_{\mathbf{p}}$  abate with  $l$ , which suggests that, states with higher number of nodes, experience confinement to a greater extent.

Now Fig. 3 inscribes variation of  $R_{\mathbf{r}}^\alpha, S_{\mathbf{r}}$  ( $IE_{\mathbf{r}}$ ) and  $R_{\mathbf{p}}^\beta, S_{\mathbf{p}}$  ( $IE_{\mathbf{p}}$ ) of  $n = 10$  states with change of  $l$  in left and right columns labeled A, B. Here  $IE$  stands for Information Entropy and in what follows this is loosely used to signify any or all of the measures discussed in this communication. These are given at five representative  $r_c$ 's namely, 0.1, 10, 60, 100,  $\infty$ , identified by (a)-(e) in parentheses. At first four finite  $r_c$ 's, both  $R_{\mathbf{r}}^\alpha$  and  $S_{\mathbf{r}}$  fall off to

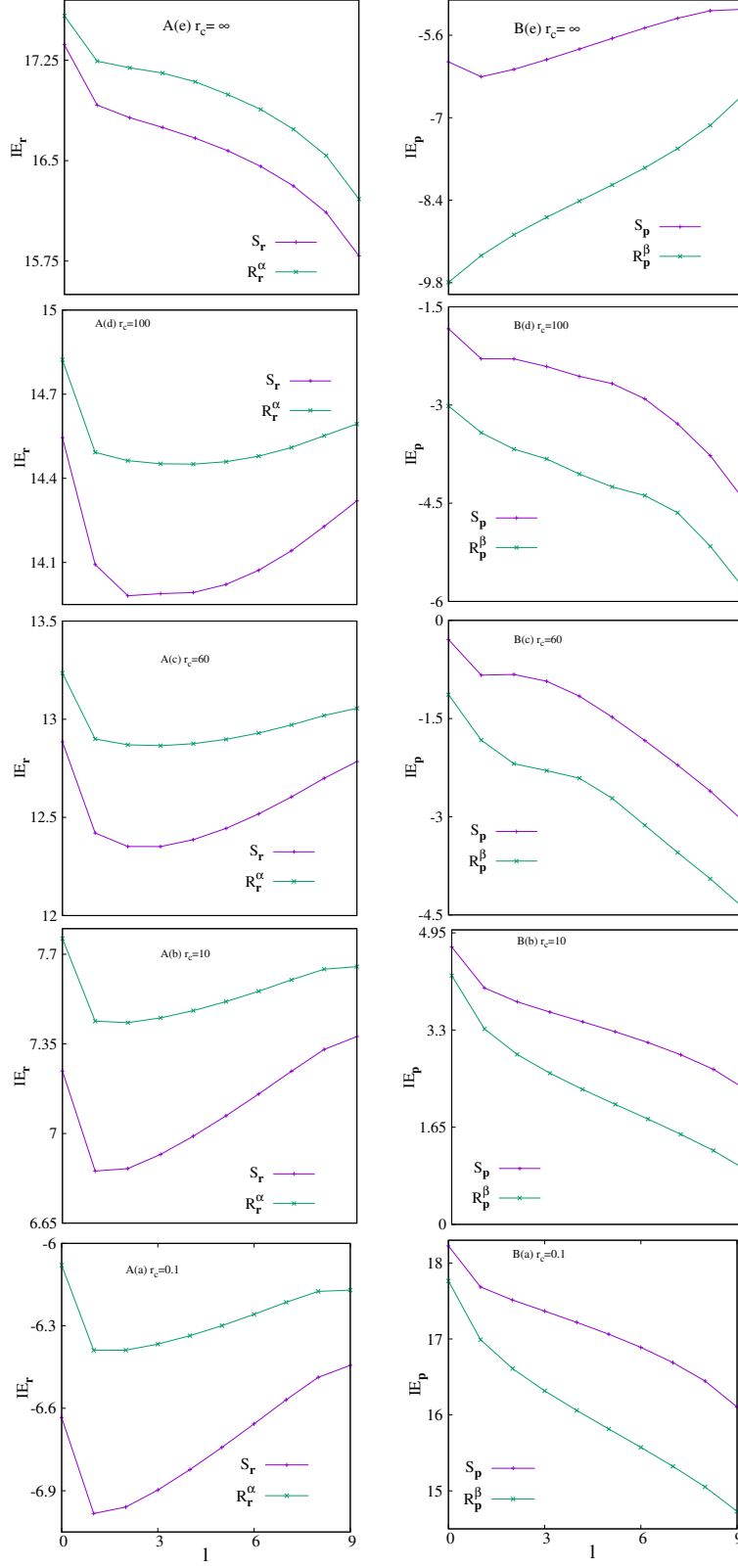


FIG. 3: Variation of  $R_r^\alpha, S_r$  ( $IE_r$ ) and  $R_p^\beta, S_p$  ( $IE_p$ ) against  $l$  for  $n = 10$  states of CHA in A and B columns. Five specific  $r_c$ 's (0.1, 10, 60, 100,  $\infty$ ) are identified in parentheses (a), (b), (c), (d), (e) respectively. See text for detail.



TABLE VII:  $E_r, E_p, E_t$  for  $2p, 3d$  states of CHA at various  $r_c$ . For more details, see text.

$r_c$	$E_r$	$E_p$	$E_t$	$r_c$	$E_r$	$E_p$	$E_t$
$2p^{\dagger}$				$3d^{\P}$			
0.1	805.746259389130	0.00000227289	0.0018313726	0.1	851.986890492579	0.00000137674	0.0011729644
0.2	101.040180954047	0.00001814520	0.0018333943	0.2	106.590831757296	0.00001100401	0.0011729266
0.3	30.0353202004482	0.00006110958	0.0018354458	0.3	31.610240295272	0.00003710446	0.0011728809
0.5	6.5311618804191	0.00028167391	0.0018396579	0.5	6.840055708558	0.00017145905	0.0011727895
0.8	1.6113769393302	0.00114576730	0.001846263	0.8	1.674574222639	0.00070026869	0.0011726519
1	0.8311099104230	0.00222698556	0.0018508698	1	0.859020100126	0.00136499761	0.0011725604
5	0.0083268168966	0.23942780273	0.0019936715	7.5	0.002245898234	0.52169438759	0.0011716725
15	0.0014334774547	1.90861683331	0.0027359592	15	0.000370433690	3.22168315792	0.00119342
25	0.0013988503823	1.97640112599	0.0027646895	50	0.00001394232	35.52898842628	0.0004953565
45	0.0013988227375	1.97576308974	0.0027637423	100	0.000172694164	7.10053419923	0.0012262208

$^{\dagger}E_r, E_p, E_t$  in FHA for  $2p$  states ( $|m| = 0$ ) are: 0.001398822737, 1.975763081024, 0.002763742330.

$^{\P}E_r, E_p, E_t$  in FHA for  $3d$  states ( $|m| = 0$ ) are: 0.000172694164, 7.1005342704468, 0.0012262208417.

reach certain minima and then improve with  $l$  in panels A(a)-A(d). Positions of both these minima shift to right as  $r_c$  is raised. Locations of these lowest points correspond to  $l$  values in accordance with Tables II and IV discussed before. However, in  $r_c = \infty$  limit, for both measures in  $r$  space, the minima disappear; rather there is a steady decline with  $l$  which passes through a plateau region. The respective  $p$ -space quantities in first four panels B(a)-B(d) on the right side, decline gradually with  $l$ . However, in top fifth panel B(e), both of them are raised with increment of  $l$ . This study simply reveals distinctly separate behavior of a H atom from free to confined environment. In case of FHA, both spread and radial nodes of an wave-function reduce with  $l$ ; hence  $R_r^\alpha$  as well as  $S_r$  diminish while  $R_p^\beta$  increases with uprise of  $l$ . Further, there appears a shallow minimum in  $S_p$  for FHA. But in the confinement scenario, there exists an interplay between two mutually opposing factors: (i) radial confinement (favoring localization) and (ii) accumulation of radial nodes with reduction in  $l$  (promoting delocalization). Hence, such minima appear in IE plots in panels A(a)-A(d) and B(a)-B(d).

Next we move on to discuss the last measure in this work, namely,  $E$  for same four non-zero  $l$  states as considered for  $R, T, S$ , in Table VII and S4 in SM. Once again no literature results could be found to compare. Generally speaking, behavior of  $E$  is usually reverse to those of  $R, T, S$  in Tables I, III, V and S1-S3. Thus for all four states,  $E_r$ 's diminish, while  $E_p$  advance with surge of  $r_c$ . As  $r_c$  approaches zero,  $E_r$  obeys the trend  $E_r(5g) > E_r(4f) >$

TABLE VIII:  $E_{\mathbf{r}}$  and  $E_{\mathbf{p}}$  for all  $l$  states corresponding to  $n = 10$ , of CHA at representative  $r_c$  values, in top and bottom sections. For more details, consult text.

$E_{\mathbf{r}}$							
$l$	$r_c = 0.1$	$r_c = 0.5$	$r_c = 1$	$r_c = 10$	$r_c = 40$	$r_c = 80$	$r_c = 100$
0	7747.631350106	62.389881644	7.861047634	0.008550277	0.0000975413	0.0000072401	0.0000029779
1	6063.245277416	48.6353842949	6.0994482170	0.00641025319	0.0000996112	0.0000094350	0.0000040864
2	4522.362533153	36.2403977184	4.5396157540	0.00470099482	0.0000773147	0.0000085650	0.0000039070
3	3530.138368622	28.2761820347	3.5399931260	0.00363570042	0.0000603524	0.0000072797	0.0000034687
4	2838.936113913	22.7331219908	2.8450195749	0.00290537538	0.0000480878	0.0000060612	0.0000029830
5	2326.540075860	18.6259402411	2.3303725215	0.00236895765	0.0000389288	0.0000050118	0.0000025222
6	1930.662444626	15.4535730094	1.9329918593	0.00195674165	0.0000318467	0.0000041310	0.0000021092
7	1618.128828159	12.9493540013	1.6193470206	0.00163196755	0.0000262324	0.0000033940	0.0000017474
8	1375.046723046	11.0013562943	1.3753245996	0.00137841885	0.0000217702	0.0000027783	0.0000014345
9	1224.322475119	9.79175302714	1.2235277207	0.00121564677	0.0000186122	0.0000022894	0.0000011795
$E_{\mathbf{p}}$							
0	0.00000001732663	0.000002159204	0.000017186150	0.01275050	0.918902	6.52106	12.55735
1	0.00000003453069	0.000004307362	0.00003435147	0.02945819	1.366699	10.40162	22.83099
2	0.00000004594109	0.000005733162	0.00004575769	0.04151677	1.479949	13.08729	25.89834
3	0.0000000570426	0.00000712045	0.00005685540	0.05313830	1.937268	15.702434	29.25821
4	0.0000000693689	0.000008660817	0.00006917634	0.06584220	2.714584	16.70624	34.56930
5	0.0000000840379	0.00001049398	0.00008383898	0.0807910	3.767910	18.52554	38.28028
6	0.0000001024152	0.00001279075	0.0001022107	0.0993984	5.123417	24.45627	43.23403
7	0.0000001266503	0.00001582009	0.0001264462	0.12388312	6.89702	37.097591	58.60068
8	0.0000001609259	0.00002010565	0.0001607428	0.1585969	9.37541	59.3034	96.4456
9	0.00000021939962	0.00002741951	0.00021930107	0.2181656	3.56075	99.301658	178.3531

$E_{\mathbf{r}}(3d) > E_{\mathbf{r}}(2p)$  which gets reversed to  $E_{\mathbf{r}}(2p) > E_{\mathbf{r}}(3d) > E_{\mathbf{r}}(4f) > E_{\mathbf{r}}(5g)$  in opposite  $r_c$  limit. Contrariwise,  $E_{\mathbf{p}}$  shows exactly opposite trend from its  $r$ -space counterpart at both small and large  $r_c$  regions. Finally, Table VIII features  $E_{\mathbf{r}}, E_{\mathbf{p}}$  for  $n = 10$  states in upper, lower portions. For all ten  $l$ ,  $E_{\mathbf{r}}$ 's collapse with accrual of  $r_c$ . **At first four  $r_c$  values  $E_{\mathbf{r}}$  droops down with rise of  $l$ . But, in other three  $r_c$  values there appear maxima at  $l = 1$ .** In  $p$  space, these patterns are completely reverse from  $r$ -space counterparts. Trends in  $E_{\mathbf{r}}, E_{\mathbf{p}}$  with respect to  $r_c$  complement the findings of  $R, T, S$ .

Figure 4 now sketches the **logarithmic** change of  $E_{\mathbf{r}}, E_{\mathbf{p}}$  with  $r_c$  for  $n = 10$  states in panels (a), (b). In contrast to  $R$  and  $S$ ,  $E_{\mathbf{r}}$  lessens whereas  $E_{\mathbf{p}}$  strengthens as  $r_c$  grows, for any given  $n, l$ . Like all other measures, they both eventually merge to their FHA values. Convergence of  $E_{\mathbf{p}}$  is not obvious from panel (b); however this can be verified upon extending  $r_c$  to some sufficiently large value. As in case of Tables VII and S4, this result again consolidates our

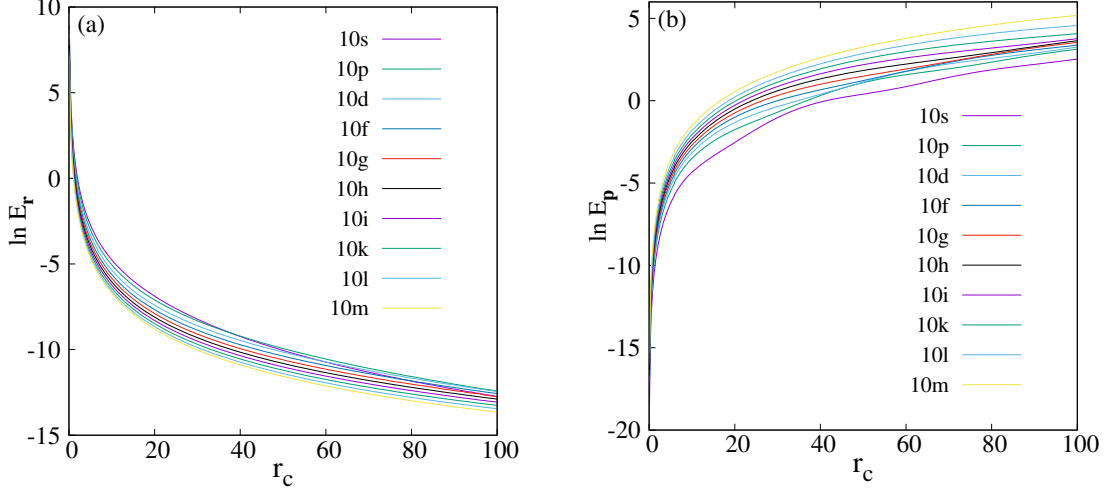


FIG. 4: Logarithmic changes of  $E_r, E_p$  of CHA with  $r_c$ , for  $n = 10$ , in panels (a), (b). Consult text for detail.

previous discussion on  $R, T, S$  that, relaxation in confinement facilitates delocalization.

Lastly in order to understand these measures with charge, Fig. 5 displays behavioral patterns of  $R, S, E$  in conjugate  $r, p$  spaces. In this occasion, we limit the discussion to ground state only, as it can be trivially extended for other states. These are followed at seven particular  $Z$ , viz., 1, 2, 3, 4, 5, 10, 15. Bottom and top rows characterizing  $r$ - $p$  space properties are denoted by A, B, while  $R, S, E$  are identified by parentheses (a), (b), (c) respectively. Note that  $T$  behavior is similar in fashion to  $R$ ; thus lead to common interpretation and hence not reported in this figure. It is seen from bottom three panels that,  $R_r^\alpha, S_r$  advance, whereas,  $E_r$  falls off with an escalation in  $Z$ . Whereas from top row it is observed that  $R_p^\beta, S_p$  decay while  $E_p$  intensifies with increment of  $Z$ . In B(c) segment,  $Z = 1, Z = 2$  graphs also show similar behavior like other  $Z$  values (not clear from panel B(c)). A careful scrutiny of these measures with respect to  $Z$  suggests that, for any arbitrary  $nl$  state, an increase in  $Z$  promotes localization. Hence, the electron density gets tightened as one goes to heavier atoms. This strengthens the trend in results of various observed chemical phenomena like *electronegativity, ionisation potential, hard-soft* interaction etc., in atomic systems. Table portraying the values of  $R, T, S, E$  at various  $Z$  are not given here. Because, such tables for  $R, T, S, E$  can easily be constructed with the help of their definition in section II and data provided in section III.

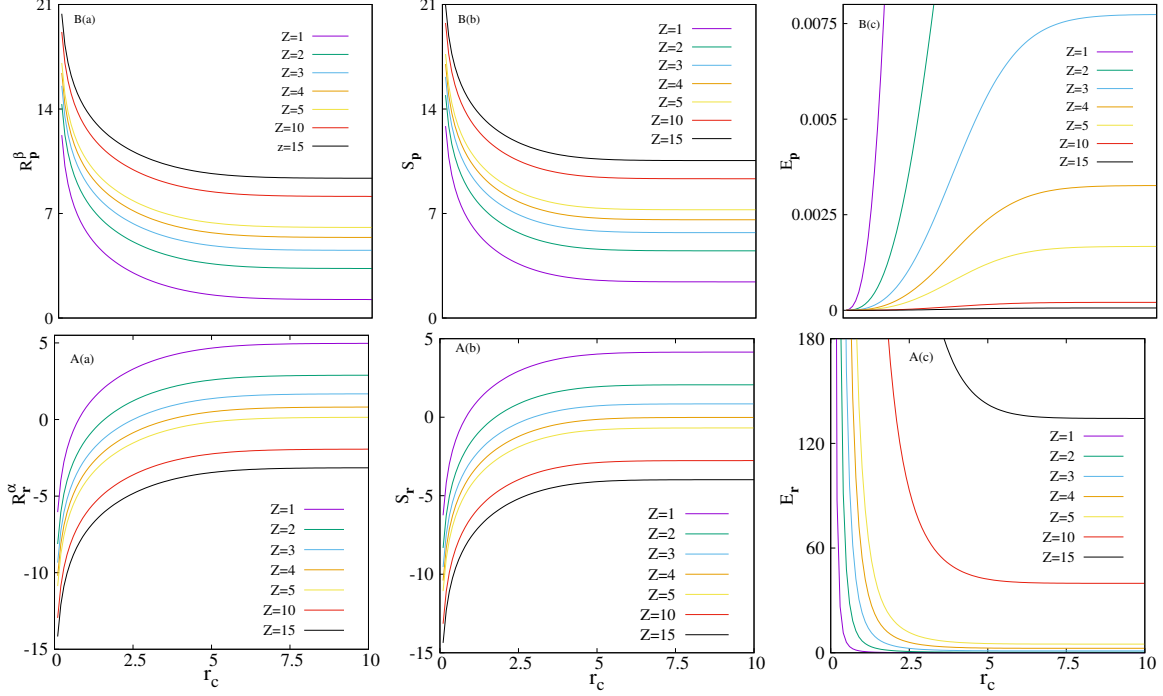


FIG. 5: Nature of  $R_{\mathbf{r}}^{\alpha}, S_{\mathbf{r}}, E_{\mathbf{r}}$  (A) and  $R_{\mathbf{p}}^{\beta}, S_{\mathbf{p}}, E_{\mathbf{p}}$  (B) in  $r$  (lower) and  $p$  (upper) spaces, for seven selected  $Z$ .  $R, S, E$  are labeled by parentheses (a), (b), (c) respectively. Ground-state results are given for  $\alpha = \frac{3}{5}, \beta = 3$ . See text for details.

#### IV. FUTURE AND OUTLOOK

Information-theoretic measures like  $R$ ,  $T$ ,  $S$ ,  $E$  are explored for  $l \neq 0$  states of CHA in both  $r$ ,  $p$  spaces. Accurate results for *combined* measures (radial *plus* angular) are provided for  $2p, 3d, 4f, 5g$  and  $n = 10$  states of CHA, keeping  $m$  fixed at zero. Except for very recent publication of  $S_{\mathbf{r}}, S_{\mathbf{p}}$  in  $2p, 3d$  states, all these quantities are reported for first time. It is found that at small  $r_c$ , with growth of  $n$ ,  $R_{\mathbf{r}}^{\alpha}, T_{\mathbf{r}}^{\alpha}$  build up while  $E_{\mathbf{r}}$  deteriorate. Beside this,  $R_{\mathbf{r}}^{\alpha}, T_{\mathbf{r}}^{\alpha}, S_{\mathbf{r}}$  pass through a minimum with addition of  $l$ . Further, an investigation on  $n = 10$  states has been made to get an idea about the high-lying states of CHA. It is realized that, they may be exploited to analyze the spread as well as diffused nature of Rydberg-hydrogenic states. Additionally, scaling property has been utilized to ascertain the effect of *atomic number* on IE of confined atomic systems. Actually, upgradation in  $Z$  strengthens the  $r$ -space electron density of any arbitrary  $nl$  state of CHA. An examination of these quantities in the realm of Rydberg states under various types of confined environment may be worthwhile to consider. A collateral inspection of many-electron atomic systems

regarding IE and periodic properties would be highly desirable.

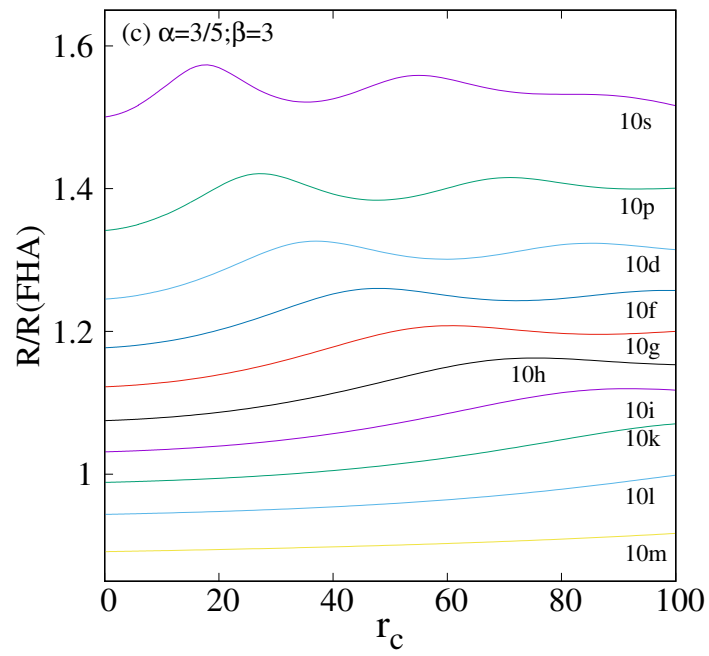
## V. ACKNOWLEDGEMENT

Financial support from DST SERB, New Delhi, India (sanction order: EMR/2014/000838) is gratefully acknowledged. NM thanks DST SERB, New Delhi, India, for a National-post-doctoral fellowship (sanction order: PDF/2016/000014/CS).

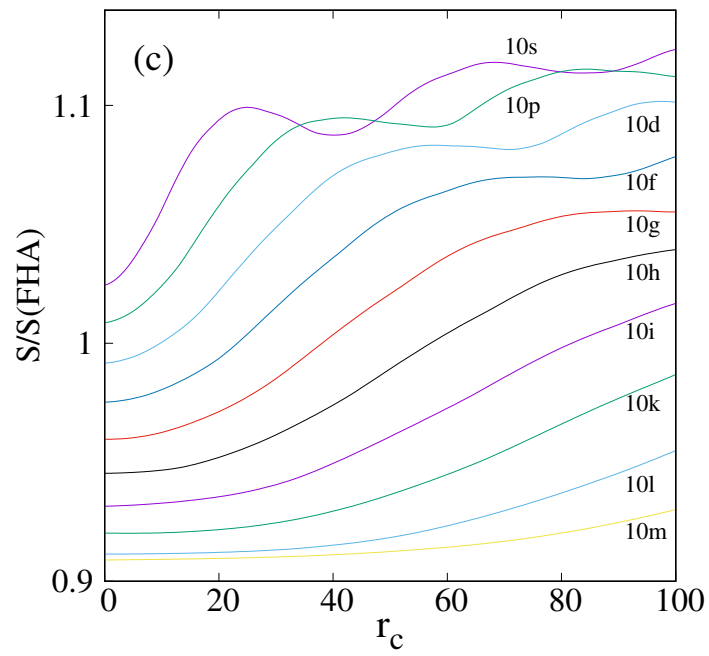
- 
- [1] N. Mukherjee and A. K. Roy, *Int. J. Quant. Chem.* (accepted).
  - [2] S.-Y. Ch'en and M. Takeo, *Rev. Mod. Phys.* **29**, 20 (1957).
  - [3] W. Jaskólski, *Phys. Rep.* **271**, 1 (1996).
  - [4] J. R. Sabin, E. Brändas and S. A. Cruz (Eds.), *The Theory of Confined Quantum Systems*, Parts I and II, *Advances in Quantum Chemistry*, Vols. 57 and 58 (Academic Press, 2009).
  - [5] J. Katriel and H. E. Montgomery Jr., *J. Chem. Phys.* **137**, 114109 (2012).
  - [6] K. D. Sen (Ed.), *Electronic Structure of Quantum Confined Atoms and Molecules*, (Springer, Switzerland, 2014).
  - [7] H. Pang, W-S. Dai and M. Xie, *J. Phys. A* **44**, 365001 (2011).
  - [8] A. Michels, J. de Boer and A. Bijl, *Physica* **4**, 981 (1937).
  - [9] N. Aquino, A. Flores-Riveros and J. F. Rivas-Silva, *Phys. Lett. A* **377**, 2062 (2013).
  - [10] L. G. Jiao, L. R. Zan, Y. Z. Zhang and Y. K. Ho, *Int. J. Quant. Chem.* **117**, e25375 (2017).
  - [11] N. Sobrino-Coll, D. Puertas-Centeno, I. V. Toranzo and J. S. Dehesa, *J. Stat. Mech.* **8**, 083102 (2017).
  - [12] D. Puertas-Centeno, N. M. Temme, I. V. Toranzo and J. S. Dehesa, *J. Math. Phys.* **58**, 103302 (2017).
  - [13] S. Goldman and C. Joslin, *J. Phys. Chem.* **96**, 6021 (1992).
  - [14] N. Aquino A., *Int. J. Quant. Chem.* **54**, 107 (1995).
  - [15] J. Garza, R. Vargas and A. Vela, *Phys. Rev. E* **58**, 3949 (1998).
  - [16] C. Laughlin, B. L. Burrows and M. Cohen, *J. Phys. B* **35**, 701 (2002).
  - [17] B. L. Burrows and M. Cohen, *Int. J. Quant. Chem.* **106**, 478 (2006).
  - [18] N. Aquino, G. Campoy and H. E. Montgomery Jr. , *Int. J. Quant. Chem.* **107**, 1548 (2007).

- [19] D. Baye and K. D. Sen, Phys. Rev. E **78**, 026701 (2008).
- [20] H. Ciftci, R. L. Hall and N. Saad, Int. J. Quant. Chem. **109**, 931 (2009).
- [21] H. E. Montgomery and K. D. Sen, Phys. Lett. A **376**, 1992 (2012).
- [22] R. Cabrera-Trujillo and S. A. Cruz, Phys. Rev. A **87**, 012502 (2013).
- [23] A. K. Roy, Int. J. Quant. Chem. **115**, 937 (2015); *ibid.*, **116**, 953 (2016).
- [24] A. Solórzano, N. Aquino and A. Flores-Riveros, Can. J. Phys. **94**, 894 (2016).
- [25] G.-H. Sun, M. A. Aoki and S.-H. Dong, Chin. Phys. B **22**, 050302 (2013).
- [26] G.-H. Sun, S.-H. Dong and N. Saad, Ann. Phys. (Berlin) **525**, 934 (2013).
- [27] W. A. Yahya, K. J. Oyewumi and K. D. Sen, Int. J. Quant. Chem. **115**, 1543 (2015).
- [28] S. Dong, G.-H. Sun, S.-H. Dong and J. P. Draayer, Phys. Lett. A **378**, 124 (2014).
- [29] R. Valencia-Torres, G.-H. Sun and S.-H. Dong, Phys. Scr. **90**, 035205 (2015).
- [30] G.-H. Sun, P. Duan, C.-N. Oscar and S.-H. Dong, Chin. Phys. B **24**, 100303 (2015).
- [31] G. Yañez-Navarro, G.-H. Sun, T. Dytrych, K. D. Launey, S.-H. Dong and J. P. Draayer, Ann. Phys. **348**, 153 (2014).
- [32] X.-D. Song, G.-H. Sun and S.-H. Dong, Phys. Lett. A **379**, 1402 (2015).
- [33] G.-H. Sun, S.-H. Dong, K. D. Launey, T. Dytrych and J. P. Draayer, Int. J. Quant. Chem. **115**, 891 (2015).
- [34] N. Mukherjee, A. Roy and A. K. Roy, Ann. Phys. (Berlin) **527**, 825, (2015).
- [35] N. Mukherjee and A. K. Roy, Ann. Phys. (Berlin) **528**, 412, (2016).
- [36] A. Ghosal, N. Mukherjee and A. K. Roy, Ann. Phys. (Berlin) **528**, 796, (2016).
- [37] K. Ch. Chatzisavvas, Ch. C. Moustakidis and C. P. Panos, J. Chem. Phys. **123**, 174111 (2005).
- [38] E. Romera and Á. Nagy, Phys. Lett. A **372**, 4918 (2008).
- [39] A. Grassi, Int. J. Quant. Chem. **108**, 774 (2008).
- [40] N. Flores-Gallegos, Chem. Phys. Lett. **666**, 62 (2016).
- [41] I. Varga and J. Pipek, Phys. Rev. E **68**, 026202 (2003).
- [42] R. Renner, N. Gisin and B. Kraus, Phys. Rev. A **72**, 012332 (2005).
- [43] P. Lévy, S. Negy and J. Pipek, Phys. Rev. A **72**, 022302 (2005).
- [44] F. Verstraete and J. I. Cirac, Phys. Rev. B **73**, 094423 (2006).
- [45] A. Bialas, W. Czyz and K. Zalewski, Phys. Rev. C **73**, 034912 (2006).
- [46] L. L. Salcedo, J. Math. Phys. **50**, 012106 (2009).
- [47] S.-B. Liu, C.-Y. Rong, Z.-M. Wu and T. Lu, Acta. Phys.-Chim. Sin. **31**, 2057 (2015).

- [48] M. Gell-Mann and C. Tsallis (Eds.), *Nonextensive Entropy-Interdisciplinary Applications*, Chapter I, (Oxford University Press, 2004).
- [49] J. Naudts, *Generalised Thermostatistics*, Springer, London, 2011.
- [50] A. R. Plastino and A. Plastino, Braz. J. Phys. **29**, 79 (1999).
- [51] J. Chen and G. Li, Entropy **16**, 3009 (2014).
- [52] Á. Nagy, Int. J. Quant. Chem. **115**, 1392 (2015).
- [53] Y. L. He, Y. Chen, J. N. Han, Z. B. Zhu, G. X. Xiang, H. D. Liu, B. H. Ma and D. C. He, Euro. Phys. J. D **69**, 283 (2015).
- [54] L. D. Site, Int. J. Quant. Chem. **115**, 1396 (2015).
- [55] D. R. Alcoba, A. Torre, L. Lain, G. E. Massaccesi, O. B. Oña, P. W. Ayers, M. V. Raemdonck, P. Bultinck and D. V. Neck, Theor. Chem. Acc. **135**, 153 (2016).
- [56] N. Flores-Gallegos, Chem. Phys. Lett. **650**, 57 (2016).
- [57] S. H. Patil, K. D. Sen, N. A. watson and H. E. Montgomery Jr., J. Phys. B **40**, 2147 (2007).
- [58] A. K. Roy, J. Phys. G **30**, 269 (2004).
- [59] K. D. Sen and A. K. Roy, Phys. Lett. A **357**, 112 (2006).
- [60] A. K. Roy, Int. J. Quant. Chem. **113**, 1503 (2013); *ibid.*, **114**, 383 (2014).
- [61] C. Tsallis, J. Stat. Phys. **52** 479 (1988).







# Supplemental Materials: Information-entropic measures for non-zero $l$ states of confined hydrogen-like ions

TABLE S1: Rényi entropies,  $R_{\mathbf{r}}^{\alpha}$ ,  $R_{\mathbf{p}}^{\beta}$  and  $R_t^{(\alpha,\beta)}$  for  $4f$ ,  $5g$  states of CHA at selected  $r_c$  values, with  $\alpha = \frac{3}{5}$  and  $\beta = 3$ . See text for details.

$r_c$	$R_{\mathbf{r}}^{\alpha}$	$R_{\mathbf{p}}^{\beta}$	$R_t^{(\alpha,\beta)}$	$r_c$	$R_{\mathbf{r}}^{\alpha}$	$R_{\mathbf{p}}^{\beta}$	$R_t^{(\alpha,\beta)}$
$4f^{\dagger}$				$5g^{\P}$			
0.1	-6.09881032904	13.5563109	7.4575006	0.1	-6.09675536829	13.8239214	7.7271660
0.2	-4.01952824354	11.4774071	7.4578789	0.2	-4.01733601542	11.7448104	7.7274744
0.3	-2.80329426627	10.2615533	7.4582590	0.3	-2.80096355554	10.5287473	7.7277837
0.5	-1.27114583083	8.7301707	7.4590249	0.5	-1.26853446452	8.9969400	7.7284055
0.8	0.13835780349	7.3218298	7.4601876	0.8	0.14139955294	7.5879465	7.729346
1	0.80744036310	6.6535319	7.4609723	1	0.81077543963	6.9192028	7.7299782
7.5	6.83551829516	0.655708291	7.4912265862	7.5	6.85190763173	0.90113880	7.75304643
15	8.87593577458	-1.334419688	7.5415160866	25	10.42248270185	-2.571994854	7.850487848
75	11.39155328951	-3.296164472	8.0953888175	95	12.54714379989	-4.080092197	8.467051603
100	11.39173125808	-3.296184085	8.0955471731	100	12.54745436087	-4.080121372	8.467332989

$^{\dagger}R_{\mathbf{r}}^{\alpha}$ ,  $R_{\mathbf{p}}^{\beta}$ ,  $R_t^{(\alpha,\beta)}$  in FHA for  $2p$  states ( $|m| = 0$ ) are: 11.391731416834988, -3.2961840848475106, 8.095547331987477.

$^{\P}R_{\mathbf{r}}^{\alpha}$ ,  $R_{\mathbf{p}}^{\beta}$ ,  $R_t^{(\alpha,\beta)}$  in FHA for  $3d$  states ( $|m| = 0$ ) are: 12.547737094562322, -4.080150421410378, 8.467586673151944.

TABLE S2: Tsallis entropies  $T_{\mathbf{r}}^{\alpha}$ ,  $T_{\mathbf{p}}^{\beta}$  and  $T_t^{(\alpha,\beta)}$  for  $4f$ ,  $5g$  states of CHA at various  $r_c$ , for  $\alpha$ ,  $\beta$  as  $\frac{3}{5}$  and 3 respectively. For more details, see text.

$r_c$	$T_{\mathbf{r}}^{\alpha}$	$T_{\mathbf{p}}^{\beta}$	$T_t^{(\alpha,\beta)}$	$r_c$	$T_{\mathbf{r}}^{\alpha}$	$T_{\mathbf{p}}^{\beta}$	$T_t^{(\alpha,\beta)}$
$4f^{\dagger}$				$5g^{\P}$			
0.1	-2.2819941539	0.4999999999991	-1.140997077	0.1	-2.281814882	0.4999999999995	-1.140907441
0.2	-1.9991860306	0.4999999999463	-0.9995930152	0.2	-1.998746678	0.4999999999685	-0.999373339
0.3	-1.6853746581	0.4999999993892	-0.8426873280	0.3	-1.684614841	0.4999999996420	-0.842307420
0.5	-0.9964448564	0.4999999869370	-0.4982224152	0.5	-0.994873502	0.4999999923382	-0.497436744
0.8	0.1422579964	0.4999997815714	0.0711289671	0.8	0.1454747876	0.4999998717186	0.0727373752
1	0.9530810038	0.4999991686466	0.4765397096	1	0.9576905936	0.4999995113174	0.4788448288
7.5	35.9938331267	0.3652809476268	13.1478614733	7.5	36.247017479	0.4175385840553	15.134528355
15	84.5658772343	-6.7116097699	-567.573167850	25	159.12580417	-85.199117451	-13557.37807917
75	235.6526959759	-364.23890302	-85833.8794779	95	375.59604544	-1748.9158539	-656885.8785564
100	235.6696500573	-364.25321055	-85843.4266642	100	375.64301711	-1749.0179353	-657006.3742152

$^{\dagger}T_{\mathbf{r}}^{\alpha}$ ,  $T_{\mathbf{p}}^{\beta}$ ,  $T_t^{(\alpha,\beta)}$  in FHA for  $2p$  states ( $|m| = 0$ ) are: 235.6696405610288, -364.25321044734767, -85843.4231793272.

$^{\P}T_{\mathbf{r}}^{\alpha}$ ,  $T_{\mathbf{p}}^{\beta}$ ,  $T_t^{(\alpha,\beta)}$  in FHA for  $3d$  states ( $|m| = 0$ ) are: 375.686384239036, -1749.1195832108906, -657120.411818189.

TABLE S3:  $S_r$ ,  $S_p$  and  $S_t$  for  $4f$ ,  $5g$  states of CHA at various  $r_c$  values. See text for details.

$r_c$	$S_r$	$S_p$	$S_t$	$r_c$	$S_r$	$S_p$	$S_t$
$4f^{\dagger}$				$5g^{\P}$			
0.1	-6.3455584854	14.4653	8.1198	0.1	-6.3503683331	14.8431	8.4928
0.2	-4.2663223577	12.3859	8.1196	0.2	-4.2709619968	12.7637	8.4928
0.3	-3.0501348575	11.1695	8.1194	0.3	-3.0546027165	11.5472	8.4926
0.5	-1.5180809495	9.6371	8.1191	0.5	-1.5222004720	10.0147	8.4925
0.8	-0.1087231165	8.2272	8.1185	0.8	-0.1123079582	8.6046	8.4923
1	0.5602595052	7.5579	8.1181	1	0.5570394221	7.9351	8.4921
7.5	6.5835558029	1.53173	8.11528	7.5	6.5968026117	1.89499	8.49179
15	8.6122327603	-0.460386	8.151846	25	10.1547840589	-1.581652	8.573132
75	10.8608517807	-2.14839726	8.71245452	95	12.0497760380	-2.86862362	9.18115241
100	10.8608551968	-2.14838651	8.71246868	100	12.0497927928	-2.86859762	9.18119517

$^{\dagger}S_r$ ,  $S_p$ ,  $S_t$  in FHA for  $4f$  states ( $|m| = 0$ ) are: 10.8608551994597, -2.14838651125525, 8.712468688204.

$^{\P}S_r$ ,  $S_p$ ,  $S_t$  in FHA for  $5g$  states ( $|m| = 0$ ) are: 12.0498008635736, -2.8685790066675, 9.1812218569060.

 TABLE S4:  $E_r$ ,  $E_p$ ,  $E_t$  for  $4f$ ,  $5g$  states of CHA at various  $r_c$ . For more details, see text.

$r_c$	$E_r$	$E_p$	$E_t$	$r_c$	$E_r$	$E_p$	$E_t$
$4f^{\dagger}$				$5g^{\P}$			
0.1	902.2306730117579	0.00000092547	0.0008349874	0.1	955.29622436210	0.00000066689	0.0006370775
0.2	112.8081519710870	0.00000740021	0.000834804	0.2	119.41827435154	0.00000533361	0.0006369305
0.3	33.4334274966356	0.00002496358	0.000834618	0.3	35.38507934013	0.00001799573	0.0006367803
0.5	7.2254852493440	0.00011545852	0.0008342438	0.5	7.64401596722	0.00008326490	0.0006364782
0.8	1.7654919808300	0.00047220577	0.0008336755	0.8	1.86653668200	0.00034074934	0.0006360211
1	0.9044440955343	0.00092133060	0.000833292	1	0.95578172600	0.00066512447	0.0006357138
7.5	0.0022027597662	0.37170465631	0.0008187761	7.5	0.00228068479	0.27382597673	0.0006245107
15	0.0002938424484	2.71341384867	0.0007973162	25	0.00006598823	8.79992837948	0.0005806917
75	0.0000384084606	17.97191418384	0.0006902736	95	0.00001189257	37.45698566645	0.0004454598
100	0.000038408429927	17.97194614910	0.0006902742	100	0.00001189251	37.45679452927	0.0004454553

$^{\dagger}E_r$ ,  $E_p$ ,  $E_t$  in FHA for  $4f$  states ( $|m| = 0$ ) are: 0.000038408430432, 17.97194626972933, 0.00069027424804.

$^{\P}E_r$ ,  $E_p$ ,  $E_t$  in FHA for  $5g$  states ( $|m| = 0$ ) are: 0.0000118924912048, 37.456994650567, 0.000445456979443.